HHS Public Access

Author manuscript

Dev Dyn. Author manuscript; available in PMC 2023 June 18.

Published in final edited form as:

Dev Dyn. 2011 August ; 240(8): 1889–1904. doi:10.1002/dvdy.22685.

V-ATPase-dependent ectodermal voltage and pH regionalization are required for craniofacial morphogenesis

Laura N. Vandenberg,

Ryan D. Morrie,

Dany Spencer Adams*

The Tufts Center for Regenerative and Developmental Biology, and Biology Department, Tufts University, Medford, MA 02155

Abstract

Using voltage and pH reporter dyes, we have discovered a never-before-seen regionalization of the *Xenopus* ectoderm, with cell subpopulations delimited by different membrane voltage and pH. We distinguished three courses of bioelectrical activity. Course I is a wave of hyperpolarization that travels across the gastrula. Course II comprises the appearance of patterns that match shape changes and gene expression domains of the developing face; hyperpolarization marks folding epithelium; both hyperpolarized and depolarized regions overlap domains of head patterning genes. In Course III, localized regions of hyperpolarization form at various positions, expand, and disappear. Inhibiting H^+-transport by the H^+-V-ATPase causes abnormalities in: (a) the morphology of craniofacial structures; (b) Course II voltage patterns; and (c) patterns of *sox9*, *pax8*, *slug*, *mitf*, *xfz3*, *otx2*, and *pax6.* We conclude that this bioelectric signal has a role in development of the face, thus it exemplifies an important, under-studied mechanism of developmental regulation.

Keywords

V-ATPase; ductin; neurectoderm; craniofacial development; cranial neural crest; placodes; bioelectric signaling

INTRODUCTION

Despite solid evidence for the importance of ion-based signaling during development, only Ca^{2+}-dependent signals have received extensive attention. Regulated ion flux, or bioelectricity, is a fundamental aspect of physiology, and new reporting dyes promise to reveal the roles of other ions the way Fura and Fluo dyes have done for Ca^{2+}. Accumulating evidence shows that patterning and morphogenesis require regulated bioelectrical signals (McCaig et al., 2005; Zhao et al., 2006) because they affect cell shape, proliferation, and growth (Adams et al., 2007; Blackiston et al., 2009; Levin, 2007a; Levin, 2007b; Levin, 2009; Morokuma et al., 2008a; Morokuma et al., 2008b; Sundelacruz et al., 2008;

*Corresponding author Dr. Dany Adams, 200 Boston Ave Suite 4600, Medford, MA 02155, Dany.Adams@Tufts.edu, Tel. 617-627-6204.

Sundelacruz et al., 2009). Evidence for the role of ion flux during craniofacial (CF) development includes: (a) K^+ ion flux is required for cochlear development in guinea pigs (Jin et al., 2008); (b) development of the zebrafish otic placode requires two different Na^+/K^+-ATPase genes (Blasiole et al., 2006); (c) Ca^{2+}-ATPase is required for zebrafish semicircular canal and otolith formation (Cruz et al., 2009); and (d) in fish, feedback between eye horizontal cells and retinal neurons may be mediated by a voltage-dependent extracellular proton concentration regulated by H^+-V-ATPase activity (Jouhou et al., 2007).

The H^+-V-ATPase (Fig. 1A.i) contributes to resting V_{mem} (Hinton et al., 2009) and regulates pH inside the cell (e.g. vesicle acidification) and outside (e.g. bone breakdown by osteoclasts; Fig. 1A.ii) (Nishi and Forgac, 2002). The H^+-V-ATPase proton-transporting subunit c, also known as ductin, is highly conserved among eukaryotes (NCBI Reference Sequence NP_001082675.1, see Figure 1B), indicating a fundamental role in cell physiology. Ductin binds to β1-integrin, a protein critical for cell locomotion (Lee et al., 2004), and is also required for developmentally regulated functions including anterior neural patterning (Cruciat, 2010), tadpole tail regeneration (Adams et al., 2007), and zebrafish eye development (Wang et al., 2008). Ductin is also the binding site for Human Papilloma Virus (HPV)16 subunit E5 (Disbrow et al., 2005; Finbow et al., 1991; Goldstein et al., 1991; Saito et al., 1998), and is thus a possible factor in cervical cancer (Stoppler et al., 1996). Ductin activity is, therefore, at the hub of three higher order phenomena - development, regeneration, and tumorigenesis - each of which involves regulation of differentiation and morphogenesis.

Ductin participates in bioelectrical signaling, which refers not just to action potentials, but to steady state conditions like resting potentials that carry patterning information and are instructive (Levin, 2009); ion flux directs cell behavior, it is not just a byproduct of cell physiology (Blackiston et al., 2009). V_{mem} is known to regulate membrane proteins, for example voltage gated sodium, potassium, and chloride channels; pH affects protein conformation and enzyme activity. It has recently been shown that pH may also regulate osmosis and thus osmotic pressure in cells (Zhao et al., 2009); therefore, regulated pH differences could provide motive force or establish permissive conditions for cell shape changes.

Here, we report our discovery of a never-before-seen regionalization of membrane voltage (V_{mem}) and pH in the *Xenopus* ectoderm using the voltage-reporting dye pair CC2-DMPE and $DiBAC_4(3)$. To examine possible mechanisms, we used ductin inhibitors, both chemical and molecular, as well as reagents that target V_{mem} and/or pH by ductin-independent mechanisms. Using these reagents, we present evidence that disruption of H^+-flux alters craniofacial morphogenesis, expression of craniofacial-relevant mRNAs, and bioelectrical patterns on the developing ectoderm. Finally, we present a model for how these mechanisms might be related to the biochemical pathways known to regulate CF morphogenesis (Praetorius et al., 2000).

RESULTS

Striking, dynamic, regional V_{mem} patterns occur on the surface of neurulae

To explore changes in bioelectrical phenomena during normal development of *Xenopus* embryos, we imaged endogenous V_{mem} during neurulation using the voltage-reporting dye pair CC2-DMPE and $DiBAC_4(3)$ (Blackiston et al., 2010). Still images and time lapse videos of V_{mem} in embryos developing from gastrula to tailbud stages revealed remarkable, never-before-seen patterns of relatively hyper- and depolarized subpopulations of visible ectodermal cells (hereafter referred to as compartments or regions; see Movie 1 in supplementary material). We distinguished three courses of hyperpolarization. The first was a wave that moved across the entire embryo, apparently coincident with the appearance of cilia at the blastula surface and the beginning of neurulation-related convergence and extension (Fig. 2A). Course II comprised the closure of the neural tube, distinguished by bright signal coming from the median ectoderm as the folds close over it and a somewhat dimmer signal from the lateral ectoderm; the neural folds stay relatively depolarized (Fig. 2B, green arrows). As neural tube closure ends, distinct spots and lines of hyperpolarization appeared in anterior areas that subsequently invaginated (Fig. 2B). For example, hyperpolarization marked the future stomodeum (Fig. 2B, yellow arrows), olfactory placode (Fig. 2B, lavender arrow), and the first pharyngeal fold (Fig. 2B, brown arrows), as well as the eye field (Fig. 2B, blue arrows), in advance of the invagination of the optic placode (Fig. 2B). Course III was an embryo-wide series of localized hyperpolarizations (Fig. 2C). This course was less orderly than courses I and II, with hyperpolarizations forming and spreading in multiple smaller areas (Fig. 2C, outlined in red). Interestingly, these localized events sometimes overlapped with the regions established during course II without disturbing the previously established patterns (Fig. 2C, eye outlined in blue, stomodeum outlined in yellow). Course III was coincident with the embryonic shape change from spherical to elongated.

Ductin disruption causes craniofacial abnormalities

Our previous studies revealed a role for the H^+-V-ATPase in patterning events during tail regeneration and the generation of left-right asymmetry (Adams et al., 2006; Adams et al., 2007). The H^+-V-ATPase plays a central role in the regulation of V_{mem} and pH; therefore, we tested the hypothesis that ductin is required for Course II V_{mem} patterns and the normal patterning of CF structures. We created a mutant ductin mRNA (*xduct-noTM4)*, which lacks the 4^{th} transmembrane domain (TM4), removing the proton binding site entirely. We observed that injection of *xduct-noTM4* at the 1-, 2- or 4-cell stage disrupted CF development as assayed by observation at stage 45-48 (Table 1). Importantly, we used dosages that affect CF morphogenesis but were not toxic, as would be expected if we had generally inhibited vesicular acidification; moreover, embryos had normal sizes and behavior, and, with the exception of left-right asymmetry randomization which is caused by ductin loss-of-function (LOF; Adams et al., 2006), tadpoles had no gross malformations such as abnormal dorso-anterior index (Fig. 3).

Affected organs included: jaws and branchial arches (BAs; compare Fig. 3A wildtype morphology to Fig. 3B-G,J,M,Q, red arrowheads, and Supplement 1); eyes (Fig. 3D,F-

P,S, blue arrowheads); otocysts, otoliths, and olfactory pits (Fig. 3Bii,G,L,M,Q,R, orange arrowheads). Unilaterally small heads due to the complete loss or reduction of BAs on one side was the most common phenotype (Fig. 3B,E). Abnormalities of the eyes included: pigment along the optic nerve (Fig. 3H); thickening and pigmentation of the connection between eye and brain (3G,I); ectopic lenses (Fig. 3K); abnormal shapes (Fig. 3D,G,I,K,N-P,S); ectopic pigment (Fig. 3M,P); and connection directly to the brain (Fig. 3I,J,N,P). Reduction of eyes was also seen (Fig. 3J,L). Otocysts and otoliths showed abnormalities including: malformation (Fig. 3Bii); loss (Fig. 3G,L,Q); and in a few cases, ectopic otoliths (Fig. 3R). Finally, the olfactory pits of some injected embryos were misshapen (Fig. 3Dii,I) or fused to eyes and/or brain (Fig. 3J,O,P). Duplication or hypertrophy of the brain was another observed effect (Fig. 3I,M,N,P,Q).

By examining those injected embryos in which the lineage was traced (using the YFP signal from an *xduct-YFP* fusion construct or the coinjection of β-gal with *xduct-noTM4*), we found that affected placodal organs (eyes, otic capsule, olfactory pits) were always on the injected side of the embryo. These lineage tracers were also useful to determine that *xduct* constructs were typically expressed throughout the injected side of the embryo.

Because *xduct-noTM4* inhibits the H^+-V-ATPase, which has structural as well as ion-transporter function, we decided to explore whether ductin's role in craniofacial development was specific to the effects of proton pumping or possibly related to another function. To that end, we altered V_{mem} and/or pH using ductin-independent reagents that have been characterized previously (see Table 2). *NHE3* is a gain-of-function (GOF) reagent that alkalinizes cytoplasm but does not affect V_{mem} (Praetorius et al., 2000); injection of wildtype *nhe3* caused the same CF phenotypes (CFPs) observed with *xduct-noTM4,* indicating a role for pH regulation in signaling during morphogenesis of the head and face (Table 1 and Supplemental Figure 3). *pma1.2*, a single subunit yeast proton pump that localizes to the plasma membrane where it pumps protons out of the cell, acts as a GOF reagent (Adams et al., 2007; Bowman et al., 1997), hyperpolarizing the plasma membrane and alkalinizing cytoplasm. Expression of *pma1.2*, like *nhe3*, caused the same CFPs observed with the ductin LOF construct (Table 1 and Supplemental Figure 3). We also examined the effect of overexpressing wildtype ductin *(xduct)* on CF development. This construct also produced the same CFPs observed with *xduct-noTM4* and the ductin-independent reagents (Table 1 and Supplemental Figure 3). Therefore, we conclude that the role of ductin/H^+-V-ATPase in normal CF development is related to H^+-flux; moreover, because either increasing or decreasing H^+-flux causes similar CFPs, we conclude that regulation of H^+-flux is required to maintain pH and V_{mem} within a particular range.

Ductin activity is upstream of seven key developmentally-regulated genes

To explore how ductin's function is transduced into cell behaviors required for CF morphogenesis, we injected 1 blastomere of 2-cell embryos with *xduct-noTM4* and performed wholemount in situ hybridization (WISH) using probes for gene transcripts known to be critical for CF development. We first examined the effect of altered ductin expression by looking at stage 14, when neurulation is beginning and neural crest is being specified (Nieuwkoop and Faber, 1967). We examined the expression of two CNC markers

(*xfz3* and *slug)* and a placode marker (*sox9*). As early as stage 14, we observed abnormal expression of all three markers (Fig. 4A-C), suggesting that ductin influences, either directly or indirectly, gene expression or RNA stability patterns and neural crest specification.

We also examined four CNC markers (*xfz3*, *slug*, *mitf, sox9*) and four placode markers (*sox9*, *pax8*, *pax6*, *otx2*) in stage 20+ embryos after neural crest migration has begun. We found distorted ISH patterns of *slug*, *sox9*, *pax8*, *pax6,* and *otx2* (Fig. 4D-H), and extra domains of *otx2* and *mitf* (Fig. 4H,I); in embryos co-injected with lineage tracer, the disrupted patterns were invariably on the injected side (Fig. 4G,H). These same patterns were also observed in embryos injected with wildtype *xduct* (data not shown). Although otherwise normal axial development and metamorphosis of injected tadpoles ruled out nonspecific effects of the reagents, we also confirmed this using a probe for *xnr-1*, a patterning gene not involved in CF patterning (Fig. 4J). Even in embryos that were positive on the right side for the normally left-sided *xnr-1* (the positive control for *xduct-noTM4* activity; Adams, et al., 2006), the size and shape of the *xnr-1* ISH pattern was unchanged.

Comparing WISH patterns (Fig. 4) to tadpole phenotypes (Fig. 3) revealed that ISH patterns correlated clearly with observed morphological changes, i.e. compare *pax6* expression (Fig. 4G) to the eye abnormality in figure 3J. This correspondence is consistent with the hypothesis that ductin activity is required for establishing the correct ISH patterns of CF regulators.

Ductin disruption neither decreased NC cell migration nor changed apoptosis levels.

We examined *slug* patterns to determine whether ductin disruption affects the ability of neural crest cells to migrate into the pharyngeal arches. At all stages examined, including stages 14 and 20 mentioned above (Fig. 4B,D) and a third stage, stage 25 after neural crest cells have populated the arches, we find evidence of migration including normal population of the arches in addition to ectopic expression of the marker (Fig. 4K). We also examined the same stages for evidence of differences in apoptosis, using both a TUNEL assay and IHC for caspase, and found no difference in the number of apoptotic cells on the control vs the *xduct-noTM4* injected sides (data not shown). We conclude that the effect of ductin inhibition is not a general effect on CNC migration or apoptosis, but rather a specific effect on the WISH patterns of CNC and craniofacial placode markers, as early as stage 14.

Ductin activity is required just prior to and during neural tube closure

Alterations in gene expression in embryos expressing *xduct-noTM4* were observed as early as st. 14, suggesting that H^+-flux influences development at or prior to that stage. To explore the critical time period for ductin activity, we exposed dishes of embryos to the highly specific ductin inhibitor concanamycin beginning at different embryonic stages and lasting for different durations. Once embryos had reached st. 45-46, we counted the number of individual tadpoles that displayed one or more CFPs (Fig. 5). We found that concanamycin caused CFPs if embryos were exposed from stage 13 to stage 16, i.e. during the formation of the neural plate and folds. Exposures ending before stage 13 or starting after stage 16 did not induce CFPs, suggesting that concanamycin/H^+-flux inhibition affects induction and/or specification of CNC or placodes, but not differentiation of these cell types.

To provide more conclusive evidence that st. 13-16 are the critical ones for the effects of ductin activity on craniofacial morphogenesis, we examined the expression of *sox9*, *slug*, and *xfz3* in concanamycin-treated embryos using WISH. First, we exposed embryos to concanamycin from st. 13-14 and examined these markers at st. 14-15, at the end of the treatment period. We observed that the expression of all three genes was disrupted by concanamycin treatment (Figure 5B.i).

We also exposed embryos to concanamycin from st. 14-16, and then examined the expression of the same genes at st. 20+ after neural crest migration has begun. Again, we observed abnormal expression of *sox9*, *slug*, and *xfz3* in concanamycin-treated embryos (Figure 5B.ii), similar to the patterns observed in *xduct-noTM4-* injected embryos. From these data, we conclude that stages 13-16 are the critical ones for the effects of H^+-flux on the expression of CNC and craniofacial placode markers.

During neurulation the superficial ectoderm stains very strongly for ductin protein.

To determine whether ductin is expressed during the period of concanamycin sensitivity, we examined the localization of ductin protein during early neurula stages. As expected for a subunit of the H^+-V-ATPase, ductin was expressed throughout the neurulating embryo; the strongest signal localized to the superficial layer of the ectoderm (Fig. 6). Ductin is also expressed in the deep ectodermal cells that will become neural crest and placodes, but localization in this region is much weaker than the expression in the superficial ectoderm. These results suggest that ductin exerts its influence locally, but the effects of ductin activity on developing neural crest and placodes may be non-autonomous.

Ductin is necessary for normal pH and V_{mem} patterning

Our imaging of V_{mem} domains in untreated embryos showed that there was consistent overlapping between the hyperpolarized or depolarized regions of Course II and domains of head patterning genes such as *eya1* and *sema4A*; thus, we focused further analysis on this pattern. To address whether domains of hyperpolarized V_{mem} would correspond with alkaline pH domains, as predicted by the function of H^+-V-ATPase, we imaged embryos in BCECF dye, a pH reporter. We observed that the distribution of iso-pH compartments produced overlapping patterns to those obtained with the V_{mem} reporter dyes (compare Fig. 7A to 7B). A correspondence between high pH and hyperpolarization was predicted by the fact that H^+-V-ATPase-dependent proton efflux hyperpolarizes membranes and alkalinizes the cytoplasm. Thus these data are consistent with the hypothesis that these electrophysiological conditions are both ductin-dependent.

To test whether alterations in ductin influence these patterns, we imaged pH and V_{mem} domains in embryos injected with *xduct-noTM4*. In the majority of injected embryos we examined (9/13), course II hyperpolarization domains and pH patterns were disrupted. In every embryo with an abnormal pH or V_{mem} pattern, the disrupted side subsequently developed abnormal CF morphology (Fig. 7C,D). This indicates that ductin is a necessary determinant of bioelectrical patterns that influence the ISH patterns of CF related genes and correlate with the morphology of craniofacial tissues.

We conclude that normal craniofacial patterning includes dynamic ectodermal cell compartments defined by specific, ductin-dependent V_{mem} and pH. Divergence of these characters affects the expression of well characterized craniofacial markers and correlates strongly with changes to the shapes of CNC and placode derived structures. Because hyperpolarizations during the latter half of course II so conspicuously predicted the position of imminent shape changes, our data provide suggestive evidence that these compartments are relevant to morphogenetic movements.

DISCUSSION

We have: [1] discovered dramatic patterns of pH and V_{mem} changes in the ectoderm during *Xenopus* CF development; [2] shown for the first time that alterations in H^+ flux can alter development of BAs, jaws, otoliths, otocysts, eyes, and olfactory pits, all derivatives of CNC and placodes; [3] determined that ductin is required for this process; and [4] identified an effect of ductin disruption on the expression patterns of important head patterning genes.

Our most exciting observations were that during neurulation, remarkable, dynamic ectodermal domains of hyperpolarized cells appear just prior to and throughout important CF morphogenesis events. H^+-V-ATPase is implicated in these events because inhibition of ductin changes voltage and pH patterns and causes subsequent, spatiotemporally-correlated CF abnormalities (Fig. 7C,D). Immunohistochemistry shows that ductin is concentrated in all SE cells, not just in those localized to hyperpolarized domains. Further, our injections of *xduct-noTM4* did not specifically target ectodermal cells and therefore altered H^+-flux is expected throughout the cells on the injected side of the embryo. Yet the effects of *xduct-noTM4* are fairly specific to craniofacial structures (Fig. 3), consistent with the higher concentration of ductin in the SE (Fig. 6). As part of the H^+-V-ATPase, ductin is required for the acidification of intracellular vesicles such as lysosomes, and, in some cells, such as osteoclasts, for extracellular acidification. Our data show that ductin also has a developmentally regulated role in CF morphogenesis, raising important questions about how ductin, like proteins that control calcium or cAMP signaling, can be required in all cells for essential physiological functions, yet *also* be required for developmentally regulated, tissue specific events (Semenov et al., 2007; Ducibella et al., 2006). One hypothesis is that the physiological requirement for ductin varies, and is low during the stages when the developmental requirement for ductin is high. Indeed, developmentally regulated events are much more sensitive to ductin inhibition, as evidenced by the lack of overall toxicity of LOF treatments.

Interestingly, processing of yolk to provide nutrients for differentiating tissues also requires H^+-V-ATPase-dependent acidification (Fagotto and Maxfield, 1994), thus there could be an autonomous effect of H^+-V-ATPase. Small decreases in pH cause partial processing of yolk and larger changes cause rapid degradation due to increased activity of proteolytic enzymes (Fagotto, 1995). The location of acidified yolk platelets correlates with differentiating ectodermal tissues. Additionally, at tailbud stages, consumption of yolk platelets via acidification occurs in the arch and oral endoderm but not in morphologically static tissues (Jorgensen et al., 2009). Our data are therefore consistent with ductin regulating activity of SE cell surface proteins, and/or increasing the availability of yolk to SE cells. The

elaborate pattern of pH regionalization suggests that this mechanism of regulation can be quite intricate.

Other constructs that affected pH and V_{mem} (*pma1.2*) or pH alone (*nhe3*) also caused CFPs. Thus regulation of pH is required for development of CNC and placode derived structures. This is consistent with other work investigating effects of pH, particularly alkalinization being required for anterior neural fate (Sater et al., 1994; Uzman et al., 1998). Importantly, that the same CFPs are caused by ductin-independent H^+-flux-altering reagents suggests that H^+-flux is the important factor regulating craniofacial morphogenesis, and not ductin itself. These results also indicate that the effects of ductin on CF development could not be due to other unidentified ductin-specific factors such as binding partners or nucleotide signaling.

To further explore the relationships among bioelectrical phenomenon and known differentiation and morphogenesis cascades, we compared course II V_{mem} patterns to published data on the expression patterns of other genes involved in cranial neural crest and placode development. We found that the expression pattern of semaphorin 4A overlaps the stage 19 horseshoe (Fig. 2B brown arrows) and the dorsolateral domains of hyperpolarization (Fig. 2B orange arrows) particularly well. Semaphorins are expressed dynamically in areas where morphogenetic cell movements such as neural crest migration occur; *Sema4A* also stains neurogenic placodes in slightly older embryos (Koestner et al, 2008). We also noted that the neurula-stage expression domains of *eya1* and *six1*, markers of pre-placodal ectoderm, overlap the hyperpolarized regions of the neural tube (Fig. 2B green arrows) and the anterior semi-circle/pre-placodal area (Fig. 2B brown arrows; to aid in comparison, the arrows in figure 2 are, to a large extent, colored to match the placode maps of Schlosser and Ahrens [2004]).

In addition to the overlapping domains of hyperpolarization and CF-relevant genes, we also observed that hyperpolarized regions closely corresponded to the morphological development of specific CF structures. For example, an intense domain of hyperpolarization corresponds to the developing stomodeum, distinguishing these cells from neighboring cells that will not contribute to this structure (Fig. 2B,C). In this way, the bioelectrical patterns we observed demarcate ‘progenitor fields,’ i.e. regions of the embryo comprised of cells whose progeny will produce a specific morphological feature, and can be distinguished from neighboring cells or regions (Davidson, 1993). However, the boundary characteristics of these regions may be less restrictive than the classically understood progenitor fields defined by Davidson, as we observed waves of hyperpolarization during course III that crossed, without disturbing, the boundaries of hyperpolarized domains established during course II (Fig. 2C).

Interestingly, most of the course II hyperpolarized areas also undergo epithelial bending, i.e. the closing of the neural tube and the invagination of the olfactory, lens and otic placodes. While hyperpolarized regions overlap areas where cells are folding and changing shape, we also provide evidence that manipulating H^+-flux alters cell shape and size. We observed that cells receiving *xduct-noTM4* often appear to be oversized (Fig. 4A.ii), suggesting that H^+-V-ATPase inhibition affects cell shape. Differences in pH influence osmotic pressure in cells (Zhao et al., 2009), and are likely to produce conditions where cell shape is affected

either in the treated cells or in neighboring cells due to changes in permissive states. Further connections between pH and V_{mem} via alterations in H^+-flux and their effects on cell shape and size should be explored further.

The CFPs we observed, because they are all abnormalities in derivatives of the anterior ectoderm, including brain, CNC, and cranial placodes (eyes, otoliths and olfactory bulbs), suggest that ductin acts during patterning of the anterior neural plate. Timing experiments are consistent with this hypothesis, and indicate that the critical period for ductin activity is from stage 13 to stage 16; this timing corresponds to the bioelectrical activity of courses I and II, but not III, suggesting that course III may not be related to H^+-flux. Finally, our ISH data identified CF markers that are directly or indirectly downstream of H^+-flux; these markers, *xfz3*, *slug*, *sox9, mitf*, *pax6* and *otx2,* have all been shown to be early acting members of the CNC and placode development pathways. While some of the ISH patterns we found are consistent with an effect of ductin on neural crest migration, many embryos show *slug* expression in the branchal arches and in ectopic positions, suggesting that migration is not consistently inhibited. We also found no evidence for an effect on apoptosis resulting from ductin disruption. Taken as a whole, our data indicate that ductin inhibition affects expression of these markers early during the development of anterior ectodermal derivatives as a result of changes to H^+-flux.

The *wnt/fz* pathway is known to participate in early stages of neural crest induction and, in culture, to be sensitive to bafilomycin, another potent ductin inhibitor (George et al., 2007; Hanken and Gross, 2005). Recently, it has been reported that *frizzled*-dependent planar polarity depends on V-ATPase (Hermle et al. 2010) as does *wnt* signaling (Cruciat, 2010). Moreover, the CF phenotypes produced by overexpression of *xfz3* (see figure 1 of Rasmussen et al., 2001) are phenocopied with remarkable fidelity by ductin inhibition. Our data are thus consistent with a ductin-dependent hyperpolarization/alkalinization being a mechanism to inhibit the *wnt/fz* signaling pathway outside of its normal domain. The phenotypes caused by ductin disruption are also very similar to abnormalities caused by disruption of *xfz3*, *sox9*, *otx2* and *pax6* (Gammill and Sive, 2001; Kumasaka et al., 2005; Purcell et al., 2005; Saint-Germain et al., 2004; Schlosser and Northcut, 2000); this relationship extends to other phenotypes we found including melanocyte and somite disruption and altered neural tube closure (data not shown). Thus, ductin also influences other processes controlled by these gene products, consistent with the idea that H^+-flux is an important regulator, either direct or indirect, of these proteins. Also interesting in this context is that while we found both increases and decreases in the normal areas of expression patterns for most of the markers (Fig. 4B-F), we never found a reduction in the amount of *xfz3* (Fig. 4A). One hypothesis to explain this difference that merits future attention is that *xfz3* transcription requires a particular range of H^+-V-ATPase-regulated V_{mem}/pH, and transcription cannot occur outside that range.

A growing body of literature has investigated the mechanisms by which H^+-flux (and other bioelectrical events) can regulate gene expression and cell/tissue morphology. *In vitro* studies using a wide range of differentiated and stem cells show that changes in V_{mem} alter proliferation in a cell-type specific manner (Blackiston et al., 2009). Bioelectrical fields can also dictate cell organization, orientation, growth, differentiation and migration

(Levin, 2009). And finally, intracellular ion concentrations have been shown to mediate DNA-binding of signaling molecules and can control subcellular localization of transcription factors, providing a direct link between bioelectrical phenomena and changes in gene expression (Levin, 2007b; Levin, 2009)

Model of ductin-dependent mechanisms in CNC and placode development

Figure 8 summarizes our current model of ductin's role in craniofacial development. Ductin is the proton-translocating subunit of the H^+-V-ATPase, and in that role is required for the normal, dynamic compartmentalization of electrophysiological state in the SE during early stages of neurulation (Fig. 8A). Different courses of bioelectrical activity correlate in time and space with important morphogenetic events, such as convergence and extension and the emergence of ciliated cells (course I), in-folding of the deep ectoderm into placodes (course II), and the rapid change in embryonic shape from spherical to laterally compressed (course III). We focused our analysis on the consistent pattern found during neural fold stages, when SE of the neural folds is relatively depolarized/acidic, while SE at the midline and lateral ectoderm is relatively alkaline/hyperpolarized (Fig. 7B). In neural fold SE, we believe the H^+-V-ATPase is inactive, while it is active in the other cells, leading to two electrophysiological states.

The relatively depolarized/acidic compartment of the neural fold SE affects the expression of *xfz3, slug*, *sox9, mitf*, *pax6* and *otx2* in the deep cells. SE cells in the neural groove and lateral ectoderm are relatively hyperpolarized/alkaline. This signal inhibits the expression of *xfz3* and *mitf* in the deep ectoderm. In addition, electrophysiological states could affect mechanical/physiological conditions, such as the actin cytoskeleton, that are prerequisites for morphogenetic movements. Thus, by linking gene expression to control of cell mechanics, the electrophysiological state of the cell could be the mechanism that coordinates differentiation and morphogenesis in time and space.

Conclusions

We have shown that ductin has an essential role in CF morphogenesis: 1) the location and timing of ductin expression is consistent with a role in regulating the pattern of pH and V_{mem} in the SE of neurulating embryos; 2) the locations of alkalinized/hyperpolarized cell domains overlap with the locations of CF developmental gene expression and with locations of subsequent tissue shape change; 3) ductin disruption affects the expression patterns of CF-relevant markers; 4) ductin disruption causes CF abnormalities; 5) ductin disruption phenocopies the result of *xfz3* overexpression and disruption of *xfz3*, *sox9*, *otx2* and *pax6*; 6) loss or gain of H^+-flux cause the same suite of phenotypes, consistent with a role for ductin in keeping pH/V_{mem} within a particular range. We conclude that the pH and V_{mem} - distinguished compartments of the SE of *Xenopus* neurulae are regulated by the activity of ductin/H^+-V-ATPase, and that the pH and V_{mem} of these cells regulate expression of genes involved in CF development. Because morphogenetic movements occurred in regions that were alkalinized/hyperpolarized relative to the surrounding cells, we suggest that ductin may regulate tissue shape change. Thus, we propose that the electrophysiological state of

the cell has the required characteristics of a mechanism for coordinating differentiation and morphogenesis in time and space.

EXPERIMENTAL PROCEDURES

Xenopus husbandry

Xenopus embryos were collected according to standard protocols (Sive et al., 2000), maintained in 0.1X Modified Marc's Ringers (MMR) pH 7.8, and staged according to (Nieuwkoop and Faber, 1967). At stage 45-46, after phenotypes became clearly visible, control and treated tadpoles were anesthetized with 1.5% MS-222 (tricaine) then scored for fourteen CF phenotypes.

Concanamycin treatment

1.5 mM concanamycin A (Sigma, St. Louis, MO, USA) stocks (in DMSO) was diluted to 50–150 nM in 0.1X MMR immediately prior to each experiment; at this concentration, DMSO has no apparent effect on development. Dishes of embryos were exposed to concanamycin for different durations and at different times (see Figure 4). When not in concanamycin, embryos were kept in MMR.

Constructs

Wildtype *XDUCTIN (xduct)* and a wildtype ductin with a YFP tag *(xduct-YFP)* were generated in the laboratory. In the wildtype ductin, protons enter subunit a on the cytoplasmic side and are picked up by a negatively charged glutamic acid residue in TM4 of subunit c as it rotates past; after a complete rotation, subunit c delivers the proton to a different site in subunit a, and it is released to the other side of the membrane. A third ductin construct, a truncated ductin mutant *(xduct-no TM4)* was also created in the laboratory; elimination of TM4 removes the proton binding site entirely (Nishi and Forgac, 2002). Other constructs were: *pma1.2,* single subunit yeast proton pump (Masuda and Montero-Lomeli, 2000); and *nhe3,* a sodium-hydrogen exchanger (Praetorius et al., 2000). See Table 2.

Constructs used for in situ hybridization probes included *mitf*, a component of the pigmented retinal epithelium and melanocyte development pathways (Kumasaka et al., 2005); *xfz3*, part of the neural crest, eye and inner ear induction pathways (Rasmussen et al., 2001); *otx2*, required for anterior neural patterning (Gammill and Sive, 2001); *pax8,* required for the development of the otic placode (Saint-Germain et al., 2004); *slug,* a neural crest marker (Carl et al., 1999); *sox9,* an early marker of neural crest and the otic placode (Saint-Germain et al., 2004); and *pax6,* required for olfactory and optic placodes (Purcell et al., 2005). See Table 2.

Microinjection

Xenopus embryos were injected with capped, synthetic mRNAs (Sive et al., 2000) in the animal hemisphere of early cleavage stage embryos. For examination of CFPs, 1-cell embryos, or 1 blastomere of 2- or 4-cell embryos were injected; for ISH experiments, 1 blastomere of 2-cell embryos were injected. Rhodamine-labeled dextran or Alexa647-

labeled dextran was used as lineage tracers for all experiments. In some experiments, β-gal was coinjected with *xduct-no TM4* as a lineage label.

Immunohistochemistry

Embryos were fixed in MEMFA fixative, embedded in paraffin, and sectioned on a Leica M2255 microtome. After sections were deparaffinized, endogenous peroxidases were quenched and the samples were blocked with 5% Goat serum and 1.5% milk powder, then incubated with anti-ductin antibody (Invitrogen, Carlsbad, CA). After washing, samples were incubated with horseradish peroxidase-conjugated secondary antibodies and the signal was amplified using Tyramide Amplification (Invitrogen). Controls included: primary only and secondary only treatments, and antibody pre-adsorbed against the peptide. Controls and experimentals were incubated for the same durations in all reagents.

In Situ Hybridization

One blastomere of 2-cell embryos was injected with *xduct-noTM4* and whole mount in situ hybridization (WISH) was performed (Harland, 1991). Probes were generated in vitro using DIG labeling mix (Roche). Controls included no-probe and sense probes. Chromogenic reaction times optimized the signal:background ratio of treated embryos; controls and treated embryos were incubated for the same duration. In situ hybridization (ISH) patterns were considered abnormal if the pattern on the injected side of the embryo differed obviously from the pattern on the uninjected side. Comparisons to untreated controls were also made.

Imaging V_{mem} and pH

CC2-DMPE (N-(6-chloro-7-hydroxycoumarin-3-carbonyl)-dimyristoylphosphatidyl ethanolamine) (CC2; Invitrogen) and $DiBAC_4(3)$ (bis-(1,3-dibutylbarbituric acid) trimethine oxonol) (DiBAC; Biotium) were used as a ratio pair. A 5 mM stock of CC2 was diluted 1:1000 directly into 0.1X MMR pH 7.5 (MMR). Just prior to each experiment, DiBAC stock (1.9 mM), was diluted 1:8000 in MMR. Embryos were incubated in CC2 solution for 45-60 minutes. After washing with MMR they were put into DiBAC solution for at least 45 minutes before imaging in the DiBAC solution. At the final concentrations (≤ 1:1000), DMSO has no effect on fluorescence or development of the phenotype. An Olympus BX-61 with a Hamamatsu ORCA AG CCD camera, controlled by IPLabs or MetaMorph software, was used for imaging. CC2 filters were: EX 405/20; BS 425; EM 460/50 (Chroma filter set 31036). DiBAC filters were: EX 470/20; BS 485; EM 517/23 (Chroma filter set 41001). After corrections to remove camera noise and uneven illumination, the software calculated the ratio of intensities I_{em460}/I_{em517}. The result is a picture of V_{mem}; the brighter the pixel, the more polarized the region it represents. Controls included: artificially changing V_{mem} in a known direction; using alternative dyes; leaving out one or both dyes (Adams, 2008; Adams et al., 2007; Adams et al., 2006; Blackiston et al., 2009; Morokuma et al., 2008a). To image pH, fresh BCECF-AM (stock 5mM in DMSO, stored at −20°C) was dissolved in MMR to a final concentration of 5μM (BCECF solution). Embryos were soaked in BCECF solution for 45 minutes, rinsed, then imaged in MMR. Filter sets used were EX=450/20, BS=460, EM=535/30 and EX=500/20, BS=515, EM=535/30. Metamorph was used to calculate the ratio of I_{ex490}/I_{ex440}; the result was an image in which brighter pixels

represent areas that are alkaline relative to darker areas. Except for resizing during figure preparation, no changes were made to these images, thus pixel intensity reports relative levels of V_{mem} or pH (Blackiston, et al., 2010).

Statistical Analysis

Tadpoles with one or more CF abnormality were deemed affected, regardless of which structure(s) were malformed; numbers of normal and affected experimental embryos were compared to numbers of normal and affected controls using a χ^2test with Pearson correction for increased stringency (α=0.01, minimum meaningful difference between treated and control [mmd] = 0.1). Next, a χ^2test of heterogeneity was run to determine if experiments could be pooled. If justified (α<0.05), numbers from all similar experiments were pooled and compared to controls by χ^2 with Pearson correction (α=0.05, mmd = 0.1).

Figure preparation

Photoshop™ was used to orient, scale, and improve clarity of images (not including V_{mem} or pH images). Data were neither added nor subtracted; original images are available on request.

Supplementary Material

Refer to Web version on PubMed Central for supplementary material.

Acknowledgements

The authors thank Doug Blackiston for assistance with WISH, Dayong Qiu and Shing-Ming Cheng for help making mRNA constructs, Punita Koustubhan and Amber Currier for animal husbandry, Bill Baga for administrative aid, J-P Saint-Jeannet for *sox9* and *pax8*, M. Montero-Lomeli for *pma1.2,* M. Musch for *nhe3,* C. Wright for *xnr-1*, C. Labonne for *mitf*, V. Schneider for *otx2*, P. Klein for *xfz3*, Michael Levin for constructive suggestions with experiments and the manuscript, and three anonymous reviewers. This work was supported by NIH grants K22-DE016633 (to DSA), The Russell L. Carpenter Summer Internship (to RDM), and 1F32GM087107-01 (to LNV).

Funding:

Grant sponsor: NIH; Grant number K22-DE016633 (to DSA), Grant sponsor: NIH NRSA; Grant number 1F32GM087107-01 (to LNV), and The Russell L. Carpenter Summer Internship (to RDM).

REFERENCES

Adams DS. 2008. A new tool for tissue engineers: ions as regulators of morphogenesis during development and regeneration. Tissue Eng Part A 14:1461–1468. [PubMed: 18601591]

Adams DS, Masi A, Levin M. 2007. H^+ pump-dependent changes in membrane voltage are an early mechanism necessary and sufficient to induce *Xenopus* tail regeneration. Development 134:1323–1335. [PubMed: 17329365]

Adams DS, Robinson KR, Fukumoto T, Yuan S, Albertson RC, Yelick P, Kuo L, McSweeney M, Levin M. 2006. Early, H^+-V-ATPase-dependent proton flux is necessary for consistent left-right patterning of non-mammalian vertebrates. Development 133:1657–1671. [PubMed: 16554361]

Anderson T, Sparkowski J, Goldstein DJ, Schlegel R. 1995. Vacuolar H(+)-ATPase mutants transform cells and define a binding site for the papillomavirus E5 oncoprotein. J Biol Chem 270:6830–6837. [PubMed: 7896830]

Blackiston D, Adams DS, Lemire JM, Lobikin M, Levin M. 2011. Transmembrane potential of GlyCl-expressing instructor cells induces a neoplastic-like conversion of melanocytes via a serotonergic pathway. Dis Model Mech 4:67–85. [PubMed: 20959630]

Blackiston DJ, McLaughlin KA, Levin M. 2009. Bioelectric controls of cell proliferation: Ion channels, membrnae voltage and the cell cycle. Cell Cycle 8:1–10. [PubMed: 19182532]

Blasiole B, Canfield VA, Vollrath MA, Huss D, Mohideen MA, Dickman JD, Cheng KC, Fekete DM, Levenson R. 2006 Separate Na,K-ATPase genes are required for otolith formation and semicircular canal develoment in zebrafish. Dev Biol 294:148–160. [PubMed: 16566913]

Bowes JB, Snyder KA, Segerdell E, Jarabek CJ, Azam K, Zorn AM, Vize PD. 2010. Xenbase: gene expression and improved integration. Nucleic Acids Res 38:D607–D612. [PubMed: 19884130]

Bowman EJ, O'Neill FJ, Bowman BJ. 1997. Mutations of pma-1, the gene encoding the plasma membrane H^+-ATPase of neurospora crassa, suppress inhibition of growth by concanamycin A, a specific inhibitor of vacuolar ATPases. J Biol Chem 272:14776–14786. [PubMed: 9169444]

Brugmann SA, Moody SA. 2005. Induction and specification of the vertebrate ectodermal placodes: precursors of the cranial sensory organs. Biol Cell 97:303–319. [PubMed: 15836430]

Carl TF, Dufton C, Hanken J, Klymkowsky MW. 1999. Inhibition of neural crest migration in *Xenopus* using antisense slug RNA. Dev Biol 213:101–115. [PubMed: 10452849]

Coombs GS, Yu J, Canning CA, Velt CA, Covey TM, Cheong JK, Utom V, Banerj N, Zhang ZH, Jadulco RC. et al. 2010. WLS-dependent secretion of WNT3A requires Ser209 acylation and vacuolar acidification. J Cell Science 123:3357–3367 [PubMed: 20826466]

Cruciat CM, Ohkawara B, Acebron SP, Karaulanov E, Reinhard C, Ingelfinger D, Boutros M, Niehrs C. 2010. Requirement of prorenin receptor and vacuolar H^+-ATPase-mediated acidification for Wnt signaling. Science 327:459–463. [PubMed: 20093472]

Cruz S, Shiao JC, Liao BK, Huang CJ, Hwang PP. 2009. Plasma membrane calcium ATPase required for semicircular canal formation and otolith growth in the zebrafish inner ear. J Exp Biol 212:639–647. [PubMed: 19218514]

Davidson EH. 1993. Later embryogenesis: regulatory circuitry in morphogenetic fields. Development 118:665–690. [PubMed: 7915668]

Deardorff MA, Tan C, Saint-Jeannet JP, Klein PS. 2001. A role for frizzled 3 in neural crest development. Development 128:3655–3663. [PubMed: 11585792]

Disbrow GL, Hanover JA and Schlegel R (2005). Endoplasmic reticulum-localized human papillomavirus type 16 E5 protein alters endosomal pH but not trans-golgi pH. J Virol 79, 5839–5846. [PubMed: 15827198]

Ducibella T, Schultz RM, Ozil JP. 2006. Role of calcium signals in early development. Semin Cell Dev Biol 17:324–332. [PubMed: 16580237]

Fagotto F 1995. Regulation of yolk degradation, or how to make sleepy lysosomes. J Cell Sci 108:3645–3647. [PubMed: 8719870]

Fagotto F, Maxfield FR. 1994. Changes in yolk platelet pH during *Xenopuslaevis* development correlate with yolk utilization. A quantitative confocal microscopy study. J Cell Sci 107:3325–3337. [PubMed: 7706389]

Finbow M, Pitts J, Goldstein D, Schlegel R, Findlay J. 1991. The E5 oncoprotein target: A 16-kDa channel-forming protein with diverse functions. Mol Carcinog:441–444. [PubMed: 1724370]

Gammill LS, Sive H. 2001. Otx2 expression in the ectoderm activates anterior neural determination and is required for *Xenopus* cement gland formation. Dev Biol 240:223–236. [PubMed: 11784058]

George A, Leahy H, Zhou J, Morin PJ. 2007. The vacuolar-ATPase inhibitor bafilomycin and mutant vps35 inhibit canonical wnt signaling. Neurobiol Dis 26:125–133. [PubMed: 17239604]

Goldstein DJ, Finbow ME, Andresson T, McLean P, Smith K, Bubb V, Schlegel R. 1991. Bovine papillomavirus E5 oncoprotein binds to the 16k component of vacuolar H(+)-ATPases. Nature 352:347–349. [PubMed: 1649407]

Hanken J, Gross JB. 2005. Evolution of cranial development and the role of neural crest: Insights from amphibians. J Anat 207:437–446. [PubMed: 16313386]

Harland RM. 1991. In situ hybridization: An improved whole mount method for *Xenopus* embryos. In *Xenopus laevis*: Practical uses in cell and molecular biology, vol. 36 (ed. Kay BK and Peng HB), pp. 685–695. San Diego: Academic Press.

Hermle T, Saltukoglu D, Grunewald J, Walz G, Simons M. 2010. Regulation of Frizzled-Dependent Planar Polarity Signaling by a V-ATPase subunit. Current Biology 20:1269–1276. [PubMed: 20579879]

Hinton A, Bond S, Forgac M. 2009. V-ATPase functions in normal and disease processes. Pflugers Arch 457:589–598. [PubMed: 18026982]

Hirsch N, Harris WA. 1997. *Xenopus* pax6 and retinal development. J Neurobiol 32: 45–61. [PubMed: 8989662]

Ingber DE. 2006. Mechanical control of tissue morphogenesis during embryological development. Int J Dev Biol 50:255–266. [PubMed: 16479493]

Jin Z, Ulfendahl M, Jarlebark L. 2008. Spatiotemporal loss of K^+ transport proteins in the developing cochlear lateral wall of guinea pigs with hereditary deafness. Eur J Neurosci 27:145–154. [PubMed: 18093167]

Jorgensen P, Steen JA, Steen H, Kirschner MW. 2009. The mechanism and pattern of yolk consumption provide insight into embryonic nutrition in *Xenopus*. Development 136:1539–1548. [PubMed: 19363155]

Jouhou H, Yamamoto K, Homma A, Hara M, Kaneko A, Yamada M. 2007. Depolarization of isolated horizontal cells of fish acidifies their immediate surrounding by activating V-ATPase. J Physiol 585:401–412. [PubMed: 17932147]

Koestner U, Shnitsar I, Linnemannstons K, Hufton AL, Borchers A. 2008 Semaphorin and Neuropilin Expression During Early Morphogenesis of *Xenopuslaevis*. Dev Dyn 237:3853–3863. [PubMed: 18985750]

Kumasaka M, Sato S, Yajima I, Goding CR, Yamamoto H. 2005. Regulation of melanoblast and retinal pigment epithelium development by *Xenopuslaevis* mitf. Dev Dyn 234:523–534. [PubMed: 16028277]

Larabell C, Torres M, Rowning B, Yost C, Miller J, Wu M, Kimelman D, Moon R. 1997. Establishment of the dorso-ventral axis in *Xenopus* embryos is presaged by early asymmetries in beta-catenin that are modulated by the wnt signaling pathway. J Cell Biol 136:1123–1136. [PubMed: 9060476]

Lecuit T 2008. "Developmental mechanics": Cellular patterns controlled by adhesion, cortical tension and cell division. HFSP Journal 2:72–78. [PubMed: 19404474]

Lee I, Skinner MA, Guo H-b, Sujan A, Pierce M. 2004. Expression of the vacuolar H^+-ATPase 16-kDa subunit results in the triton x-100-insoluble aggregation of beta1 integrin and reduction of its cell surface expression. J Biol Chem 279:53007–53014. [PubMed: 15466867]

Levin M 2007a. Gap junctional communication in morphogenesis. Prog Biophys Mol Biol 94:186–206. [PubMed: 17481700]

Levin M 2007b. Large-scale biophysics: Ion flows and regeneration. Trends Cell Biol 17:261–270. [PubMed: 17498955]

Levin M 2009. Bioelectric mechanisms in regeneration: Unique aspects and future perspectives. Semin Cell Dev Biol 20:543–556. [PubMed: 19406249]

Linker C, Bronner-Fraser M, Mayor R. 2000. Relationship between gene expression domains of xsnail, xslug, and xtwist and cell movement in the prospective neural crest of *Xenopus*. Dev Biol 224:215–225. [PubMed: 10926761]

Masuda CA, Montero-Lomeli M. 2000. An nh2-terminal deleted plasma membrane H^+-ATPase is a dominant negative mutant and is sequestered in endoplasmic reticulum derived structures. Biochem Cell Biol 78:51–58. [PubMed: 10735563]

McCabe KL, Bronner-Fraser M. 2009. Molecular and tissue interactions governing induction of cranial ectodermal placodes. Dev Biol 332:189–195. [PubMed: 19500565]

McCaig CD, Rajnicek AM, Song B, Zhao M. 2005. Controlling cell behavior electrically: Current views and future potential. Physiol Rev 85:943–978. [PubMed: 15987799]

Morokuma J, Blackiston D, Adams DS, Seebohm G, Trimmer B, Levin M. 2008a. Modulation of potassium channel function confers a hyperproliferative invasive phenotype on embryonic stem cells. Proc Natl Acad Sci U S A 105:16608–16613. [PubMed: 18931301]

Morokuma J, Blackiston D, Levin M. 2008b. KCNQ1 and KCNE1 K^+ channel components are involved in early left-right patterning in *Xenopus laevis* embryos. Cell Physiol Biochem 21:357–372. [PubMed: 18453744]

Nieuwkoop PD, Faber J. 1967. Normal table of *Xenopus laevis* (daudin). Amsterdam: North-Holland Publishing Company.

Nishi T, Forgac M. 2002. The Vacuolar (H^+)-ATPASES – Nature's Most Versatile Proton Pumps. Nat. Rev. Mol. Cell Biol 3:94–103. [PubMed: 11836511]

Pannese M, Polo C, Andreazzoli M, Vignali R, Kablar B, Barsacchi G, Boncinelli E. 1995. The *Xenopus* homologue of otx2 is a maternal homeobox gene that demarcates and specifies anterior body regions. Development 121:707–720. [PubMed: 7720578]

Praetorius J, Andreasen D, Jensen BL, Ainsworth MA, Friis UG, Johansen T. 2000. NHE1, NHE2, and *NHE3* contribute to regulation of intracellular pH in murine duodenal epithelial cells. American Journal of Physiology - Gastrointestinal & Liver Physiology 278:G197–206. [PubMed: 10666043]

Purcell P, Oliver G, Mardon G, Donner AL, Maas RL. 2005. Pax6-dependence of six3, eya1 and dach1 expression during lens and nasal placode induction. Gene Expr Patterns 6:110–118. [PubMed: 16024294]

Rasmussen JT, Deardorff MA, Tan C, Rao MS, Klein PS, Vetter ML. 2001. Regulation of eye development by frizzled signaling in *Xenopus*. Proc Natl Acad Sci U S A 98:3861–3866. [PubMed: 11274406]

Saint-Germain N, Lee YH, Zhang Y, Sargent TD, Saint-Jeannet JP. 2004. Specification of the otic placode depends on sox9 function in *Xenopus*. Development 131:1755–1763. [PubMed: 15084460]

Saito T, Schlegel R, Andresson T, Yuge L, Yamamoto M, Yamasaki H. 1998. Induction of cell transformation by mutated 16k vacuolar H^+-ATPase (ductin) is accompanied by down-regulation of gap junctional intercellular communication and translocation of connexin 43 in nih3t3 cells. Oncogene 17:1673–1680. [PubMed: 9796696]

Sauka-Spengler T, Bronner-Fraser M. 2008. A gene regulatory network orchestrates neural crest formation. Nat Rev Mol Cell Biol 9:557–568. [PubMed: 18523435]

Sampath K, Cheng A, Frisch A, Wright C. 1997. Functional differences among *Xenopus* nodal-related genes in left-right axis determination. Development 124:3293–3302. [PubMed: 9310324]

Sater AK, Alderton JM, Steinhardt RA. 1994. An increase in intracellular pH during neural induction in *Xenopus*. Development 120:433–442. [PubMed: 8149919]

Schlosser G 2006. Induction and specification of cranial placodes. Dev Biol 294:303–351. [PubMed: 16677629]

Schlosser G, Ahrens K. 2004 Molecular anatomy of placode development in *Xenopuslaevis*. Dev Biol 271:439–466. [PubMed: 15223346]

Schlosser G, Awtry T, Brugmann SA, Jensen ED, Neilson K, Ruan G, Stammler A, Voelker D, Yan B, Zhang C. et al. 2008. Eya1 and six1 promote neurogenesis in the cranial placodes in a soxb1-dependent fashion. Dev Biol 320:199–214. [PubMed: 18571637]

Schlosser G, Northcutt RG. 2000. Development of neurogenic placodes in *Xenopus laevis*. J Comp Neurol418:121–146. [PubMed: 10701439]

Semenov MV, Habas R, Macdonald BT, He X. 2007. Snapshot: Noncanonical wnt signaling pathways. Cell 131:1378. [PubMed: 18160045]

Shi DL, Goisset C, Boucaut JC. 1998. Expression of xfz3, a *Xenopus* frizzled family member, is restricted to the early nervous system. Mech Dev 70:35–47. [PubMed: 9510023]

Simons M, Gault WJ, Gotthardt D, Rohatgi R, Klein TJ, Shao YM, Lee HJ, Wu AL, Fang YM, Satlin LM. et al. 2009. Electrochemical cues regulate assembly of the Frizzled/Dishevelled complex at the plasma membrane during planar epithelial polarization. Nature Cell Biology 11:286–U142 [PubMed: 19234454]

Sive H, Grainger RM, Harland R. 2000. Early development of *Xenopus laevis*. Cold Spring Harbor, New York: Cold Spring Harbor Laboratory Press.

Stoppler MC, Straight SW, Tsao G, Schlegel R, McCance DJ. 1996. The E5 gene of hpv-16 enhances keratinocyte immortalization by full-length DNA. Virology 223:251–254. [PubMed: 8806560]

Sundelacruz S, Levin M, Kaplan DL. 2008. Membrane potential controls adipogenic and osteogenic differentiation of mesenchymal stem cells. PLoS One 3:e3737. [PubMed: 19011685]

Sundelacruz S, Levin M Kaplan DL. 2009. Role of membrane potential in the regulation of cell proliferation and differentiation. Stem Cell Rev Rep 5:231–246. [PubMed: 19562527]

Uzman JA, Patil S, Uzgare AR, Sater AK. 1998. The role of intracellular alkalinization in the establishment of anterior neural fate in *Xenopus*. Dev Biol 193:10–20. [PubMed: 9466884]

Wang H, Kesinger JW, Zhou Q, Wren JD, Martin G, Turner S, Tang Y, Frank MB, Centola M. 2008. Identification and characterization of zebrafish ocular formation genes. Genome 51:222–235. [PubMed: 18356958]

Wen S, Zhu H, Lu W, Mitchell LE, Shaw GM, Lammer EJ, Finnell RH. 2010. Planar cell polarity pathway genes and risk for spina bifida. Am J Med Genet A 152A:299–304. [PubMed: 20101694]

Yanfeng WA, Tan C, Fagan RJ Klein PS. 2006. Phosphorylation of frizzled-3. J Biol Chem 281:11603–11609. [PubMed: 16513654]

Zhao H, Bringas P, Chai Y. 2006. An in vitro model for characterizing the post-migratory CNC cells of the first branchial arch. Dev Dyn 235:1433–1440. [PubMed: 16245337]

Zhao Q, Ovchinnikova K, Chai B, Yoo H, Magula J, Pollack GH. 2009. Role of proton gradients in the mechanism of osmosis. The Journal of Physical Chemistry 113:10708–10714. [PubMed: 19719272]

Zimmerman SG, Thorpe LM, Medrano VR, Mallozzi CA, McCartney BM. 2010 Apical constriction and invagination downstream of the canonical Wnt signaling pathway requires Rho1 and Myosin II. Dev Biol 340:54–66. [PubMed: 20102708]

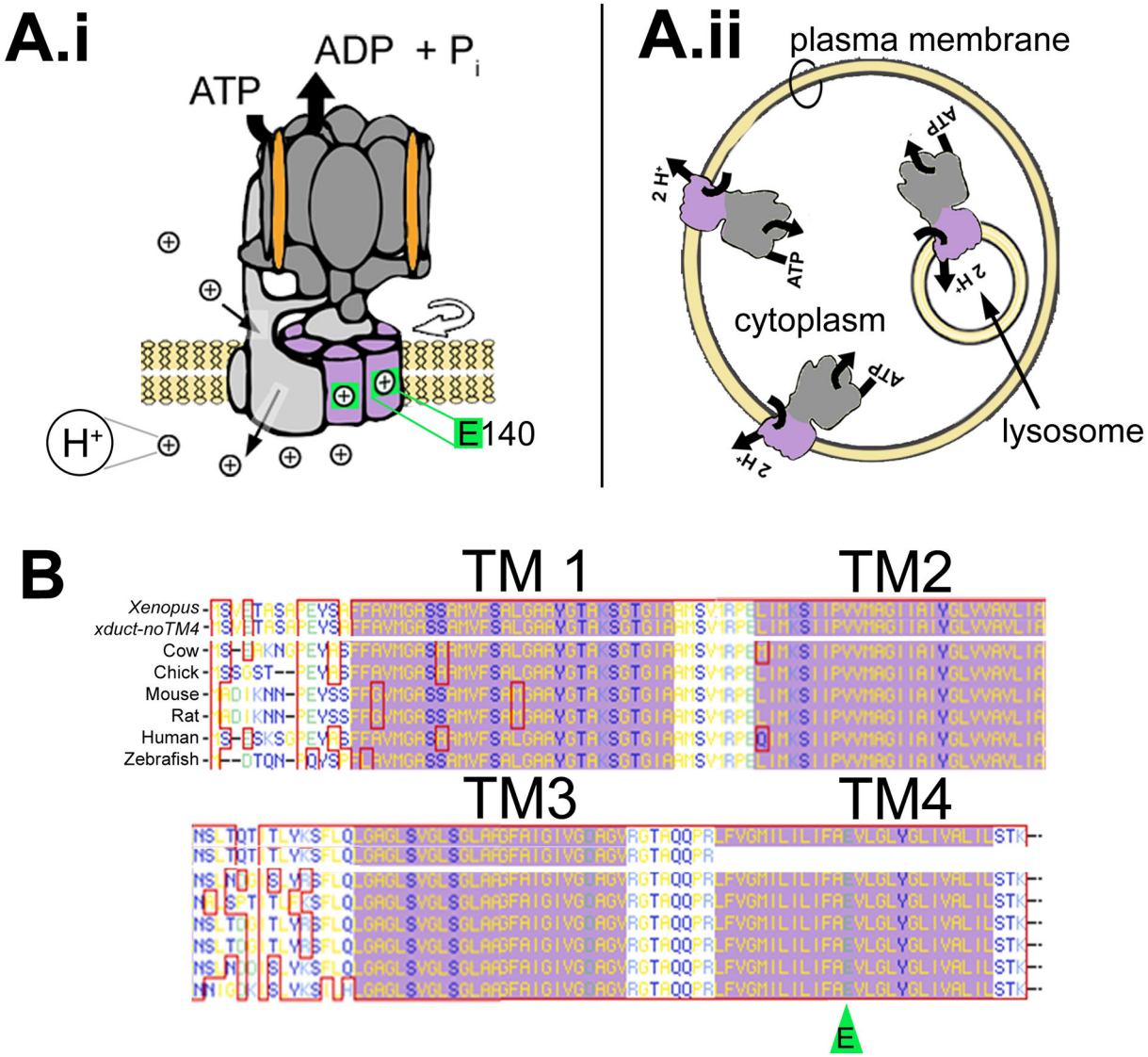

Figure 1: Ductin basics.

(A.i) Ductin (purple) is part of the transmembrane proton transporting V0 domain of the H^+-V-ATPase (Entrez Gene Name: ATPase, H^+ transporting, lysosomal 16kD, V0 subunit c; drawing after Hinton et al., 2009). The V0 domain includes a hexamer comprising four ductin monomers plus two similar proteins, c' and c''. Protons (⊕) enter subunit a on the cytoplasmic side (upper thin black arrow) and are picked up by a glutamic acid (E140, green) in TM4 of ductin. After rotation (curved, open arrow), ductin delivers the proton to another site in subunit a, which releases it to the other side of the membrane (lower thin black arrow). **(A.ii)** The H^+-V-ATPase acidifies the lumen of intracellular vesicles, including lysosomes. In some cells, it is present in the plasma membrane. (**B**) The amino acid sequence of ductin is very highly conserved. The four transmembrane domains are indicated by the purple background; the proton binding E is indicated by the green arrowhead. The top sequence is *Xenopus* ductin, the next is *xduct-noTM4*. Below that are the cow, chick, mouse, rat, human and zebrafish sequences.

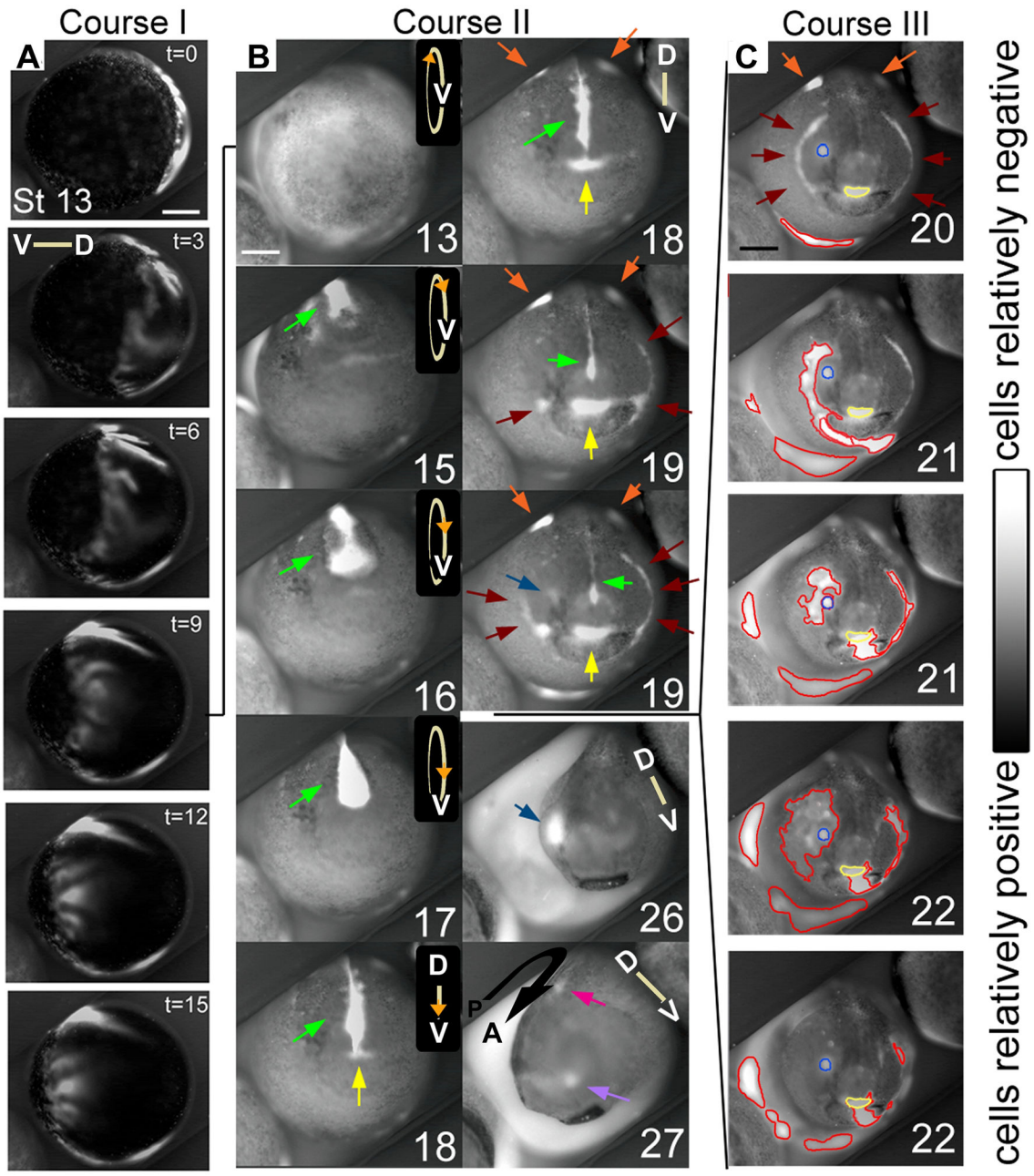

Figure 2. Regions of relatively hyperpolarized (brighter) and depolarized (darker) *Xenopus* ectodermal cells are highly dynamic from stage 13 to stage 27.

Stages are approximate due to the limitations of judging two dimensional images. Scale bars = 250 μm. Orientation of the dorsal-ventral axis is indicated by lines, except in B 13 to 17 where circles indicate that the embryo is rolling towards the viewer; the V indicates the position of the ventral side, while the orange arrowhead indicates the approximate position of the anterior pole. (**A**) Ventrolateral view of course I. A wave of hyperpolarization travels across the embryo in approximately 15 minutes, then is stationary for several minutes before disappearing. Time (t) is in minutes. (**B**) The first panel shows a ventral view of an embryo at stage 13 in which the circle of hyperpolarized cells of course I is directly visible. Course

II of the bioelectric activity begins at approximately stage 14. The visible signal emitted by the interior of the neural tube is particularly intense compared with the rest of the embryo, and changes shape between stages 14 and 19, including an hourglass at 16 to a teardrop at 17 (green arrows). At stage 18, the signal from the neural tube appears to thin. A patch of hyperpolarized cells just anterior to the neural tube signal, at the position of the stomodeum, appears, grows, then remains until approximately stage 23 (yellow arrows, and circles in C). Also at stage 18, hyperpolarized regions appear lateral to the neural folds on the dorsal side; the anterior extents of these regions are visible at the top of these images (orange arrows; see also Fig. 7A). These are visible from stage 18 until stage 21. At stage 19, lateral to the stomodeal region and apposed to the dorsolateral corners of the cement gland, foci of hyperpolarization appear, then spread as thin lines both ventrally, underlining the cement gland, and dorsally, reaching the lateral edges of the neural folds by stage 20 (brown arrows), forming a semicircle, approximately in the position of the first pharyngeal pouch. Also at stage 19, a spot of hyperpolarization appears in the right eye/olfactory placode field (blue arrow). At stage 26, the hyperpolarized spot that formed in the eye/olfactory placode area is still present, but by stage 27, that spot is much reduced and in the position of the olfactory placode (light purple arrow). A hyperpolarized spot in the approximate position of the otic placode is also visible at this stage (magenta arrow). (C) In course III, foci of hyperpolarity (circled in red) appear, spread, and disappear at different positions on the surface of the embryo, coincident with embryo stretching (compare stage 20 to stage 22). Also shown is that a course III area can spread over a course II area (blue and yellow circled areas) without disturbing it.

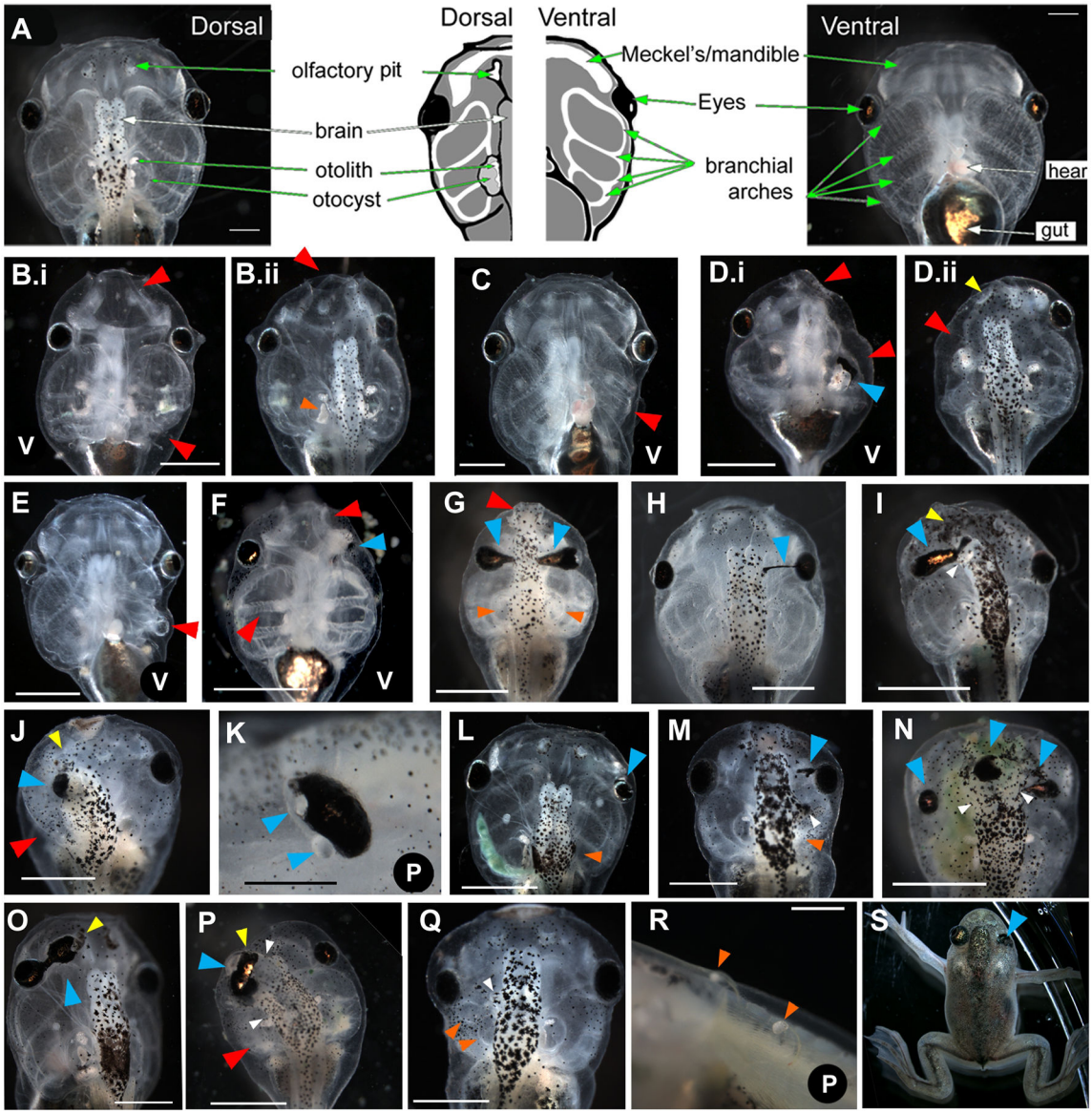

Figure 3. Range of tadpole craniofacial phenotypes caused by injection of *xduct-noTM4* at the 1, 2, or 4 cell stage.

Tadpoles were scored and imaged between stage 45 and 48. In all images, large red arrowheads (red) indicate abnormalities of jaws and branchial arches, large blue arrowheads (blue) indicate eye or pigment abnormalities, small yellow arrowheads (yellow) indicate olfactory pit abnormalities, small orange arrowheads (orange) indicate otocyst and/or otolith abnormalities, and small white arrowheads (white) indicate abnormal brain tissue. All views are dorsal except where indicated by a V (ventral) or a P (profile). Anterior is up except in panels K and R in which anterior is left and dorsal is up. All scale bars = 1 mm unless otherwise indicated. (**A**) Wildtype morphology, dorsal and ventral aspects; drawing summarizes major structures (scale bar = 500μm). (**B**) Ventral and dorsal views of a tadpole with badly malformed jaw and left branchial arches (red) as well as a malformed otolith (B.ii orange). (**C**) Ventral view of a tadpole with small left-sided branchial arches (red).

(**D**) Ventral and dorsal views of a tadpole with left-sided abnormalities of the jaw, branchial arches (red), eye, (blue) and olfactory pit (yellow). (**E**) Ventral view of malformed left-sided branchial arches (red). (**F**) Ventral view of bilateral abnormalities of the jaws and branchial arches, which lack the normal teeth (red). The left eye of this tadpole is not visible and thus abnormal (blue). (**G**) Bilateral abnormalities of the jaw (red), eyes (blue), and otoliths (orange); the branchial arches are also small. (**H**) Pigmentation of the optic nerve (blue), a commonly seen abnormality. (**I**) Thickening and pigmentation of the connection between the eye and brain (blue) is also commonly observed. This tadpole also has a malformed or missing olfactory pit (yellow) and abnormal growth of the brain (white). (**J**) Unilateral changes to the olfactory pit (yellow) eye (blue) and branchial arches (red). In this tadpole, the eye appears to be directly attached to the brain. (**K**) Eye with two lenses; it is not clear which lens is ectopic (blue). (Scale bar = 250 μm) (**L**) Embryo with a small eye (blue) and missing otocyst/otolith (orange). (**M**) Tadpole with ectopic pigment near to the eye (blue), extra brain tissue (white) and missing otocyst/otolith (orange). (**N**) Tadpole with malformed eyes and ectopic pigment along the midline (blue), as well as brain shape abnormalities (white). (**O**) Tadpole with an ectopic eye, connected to the original by a pigmented bridge (blue) that is fused with the olfactory pit (yellow). (**P**) Tadpole with left-sided abnormalities including small branchial arches (red), and a second brain (white) apparently fused to a large distorted eye (blue) and olfactory pit (yellow). (**Q**) Tadpole with small outgrowth of brain (white), a mis-formed otocyst (orange) and a missing otolith on the left side. **(R**) Ectopic otoliths growing along the dorsal midline (scale bar = 500 μm). (**S**) This froglet received *xduct-noTM4* at the one cell stage, developed into a tadpole with a malformed eye, then metamorphosed. The eye abnormality is still visible (blue).

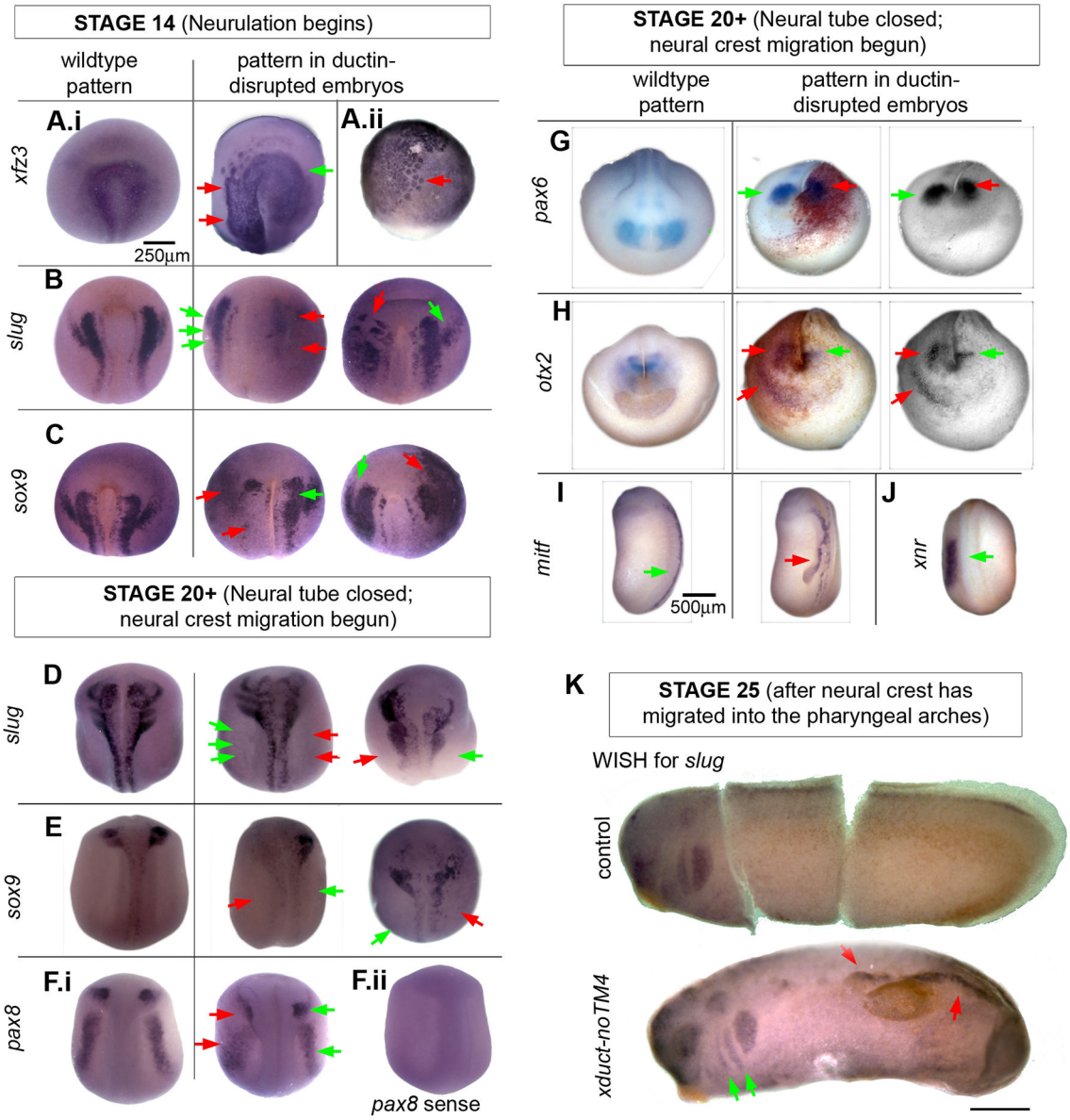

Figure 4. Wholemount in situ hybridization (WISH) indicates that ductin-dependent H^+-flux is upstream of RNAs in the CNC and placode signaling pathways.

Embryos injected with *xduct-noTM4* were probed for developmentally regulated mRNAs. In all images, red arrows point to abnormal and green to normal staining patterns. (**A-C**) Dorsal/anterior views of WISH in stage 14 embryos showing the wildtype pattern (left), an injected embryo with lower than normal expression (center), and an injected embryo with higher than normal expression (right). (**A.i**) *xfz3* a marker of neural crest; no embryos were found that had loss of *xfz3* staining on one side but were otherwise normal. (A.ii) In many *xduct-noTM4* injected specimens, cells staining positively for *xfz3* appear larger than normal at early stages (stage 10 shown). **(B)** *slug*, a marker of CNC cells. (**C**) *sox9*, at this stage a marker for otic capsule formation. (**D-H**) Embryos at stage 20. (**D**) *slug*, a marker of CNC cells; **(E)** *sox9*, a marker for otic capsule formation and CNC; **(F)** *pax8*, a marker for neural plate, otic capsule, and retina. (**F.ii**) Control using the *pax8* sense strand lacks

non-specific staining; all other sense strand controls were also negative (not shown). (**G**) Expression of *pax6*, an eye-field marker. Middle column: β-gal, used to label the injected side of the embryo, shows that the disruption to *pax6* expression is on the injected side. Right column: A red filter was placed on the camera to give a clear image of the WISH signal. (**H**) Expression of *otx2*, a marker for olfactory placode and lens. Middle and right columns as in G. Like *pax6*, *otx2* is posterior to its normal domain on the injected side. Ectopic staining is also apparent. (**I**) At stage 22, expression of *mitf*, a marker for the neural crest melanocyte lineage, is visible in a region appearing to be ectopic neural fold. (**J**) At stage 22, normal sized, one-sided expression domain of *xnr-1* in a ductin-disrupted embryo shows that ductin inhibition does not affect other patterning genes. (**K**) Stage 25 embryos stained for *slug*. The top embryo is an untreated control (cut to lay flat for imaging) showing the normal staining of slug in the pharyngeal arches. The lower embryo was injected with *xduct-noTM4* into one blastomere at the 2-cell stage. The pharyngeal arches have been populated normally, but there is ectopic staining of *slug*; both of these observations are consistent with neural crest cell motility being unaffected by ductin disruption.

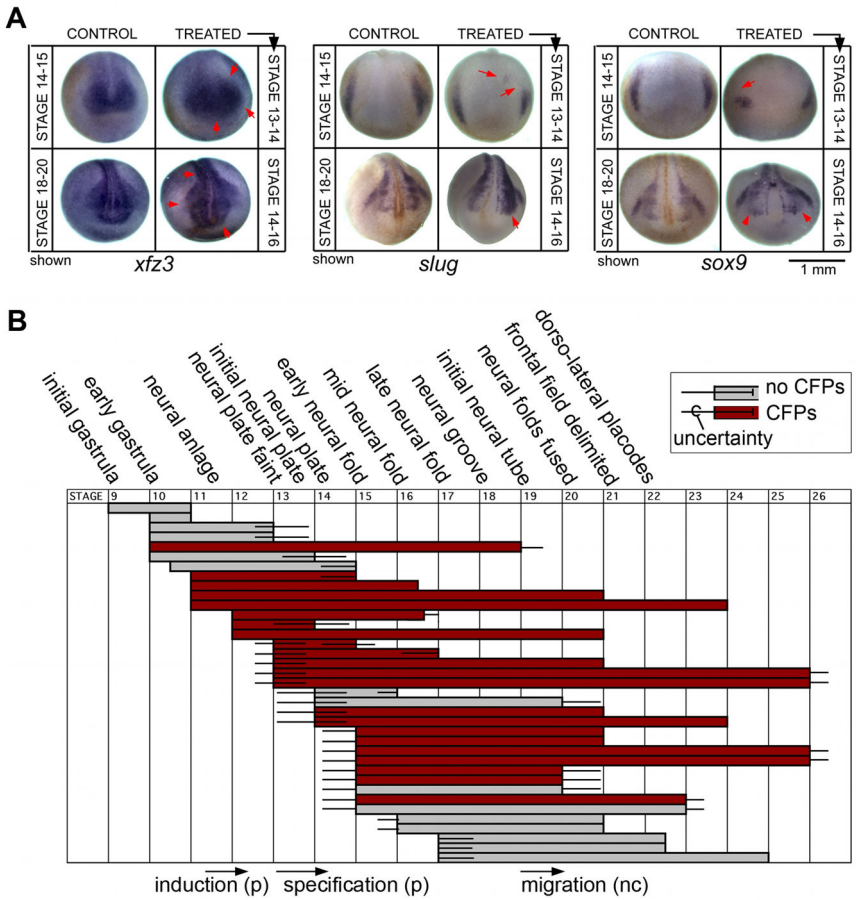

Figure 5. Inhibition of ductin by concanamycin affects WISH patterns and indicates that ductin is required during late gastrulation and early neural plate stages.

(**A**) Treatment of embryos with the highly-specific ductin inhibitor concanamycin leads to changes in the WISH patterns of *xfz3*, *slug*, and *sox9*. Like injection of *xduct-noTM4*, these changes can be seen as early as stage 14 and are still apparent at stage 20. Embryos in the top row of each panel were exposed to concanamycin from stage 13 to stage 14, then fixed at stage 14-15 for WISH; embryos in the bottom row were exposed from stage 14 to stage 16, then fixed at stage 18-20 for WISH. Timing was chosen on the basis of the concanamycin exposure experiments shown in B. (**B**) Effect of exposure to the ductin-inhibitor concanamycin at different stages (indicated on the top and bottom); each horizontal bar represents a batch of embryos treated with concanamycin; gray bars indicate that this sample did not have significantly more CFPs than the untreated control, red bars indicate a significant difference of >10% between controls and experimentals (α=0.01). Error bars represent an estimate of the uncertainty of identifying stages. Exposure to concanamycin from stage 13 to 16 caused craniofacial abnormalities.

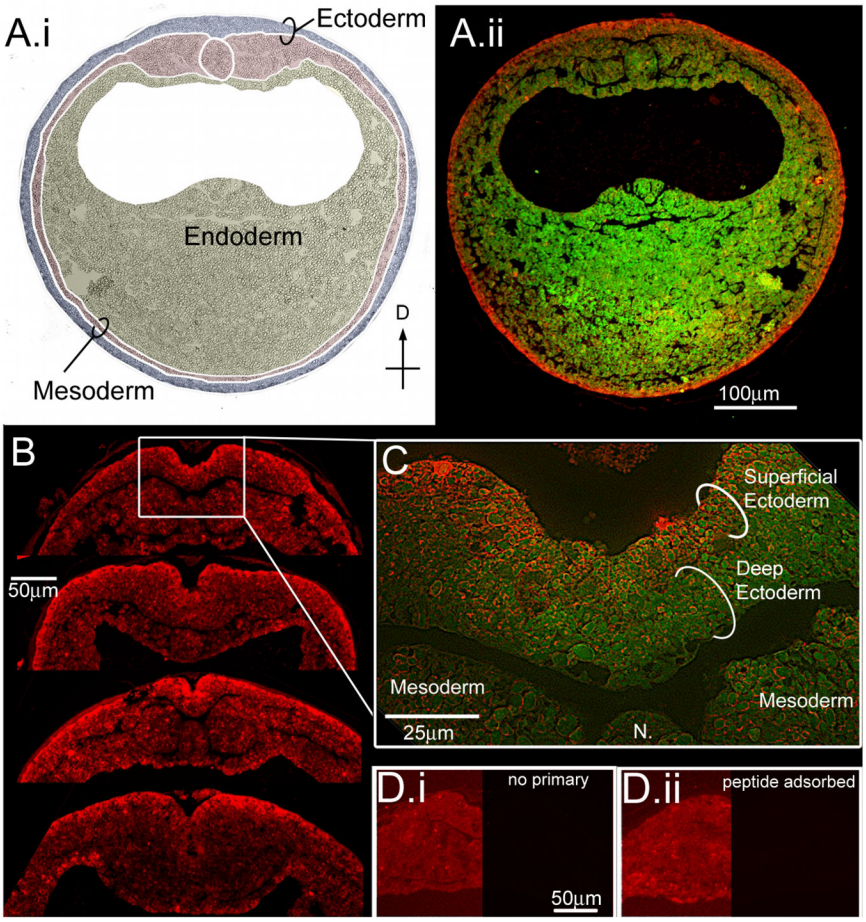

Figure 6. Ductin is present at high levels in the superficial ectoderm during neural plate stages.

(**A**) Immunohistochemistry for ductin on cross-sections from neurulating embryos. (**A.i**) Germ layers are indicated on the DIC image of the section in A.ii. (**A.ii**) Green is autofluorescence of the section, red is ductin signal. Ductin is ubiquitous, but stains most strongly in the superficial ectoderm (SE) at this stage. (**B**) Cross sections through the dorsal midline showing various configurations of the neural fold. In all sections, ductin signal is strongest in the SE. (**C**) Higher magnification shows ductin concentrated in, although not exclusively localized to, the SE. (**D.i**) Control section exposed to 2° Ab only. The left side of image has been manipulated in Photoshop to show the position of the section; right side of image shows the actual signal at same exposure as B. (**D.ii**) Control sections exposed to peptide-adsorbed antibody; sides as in D.i.

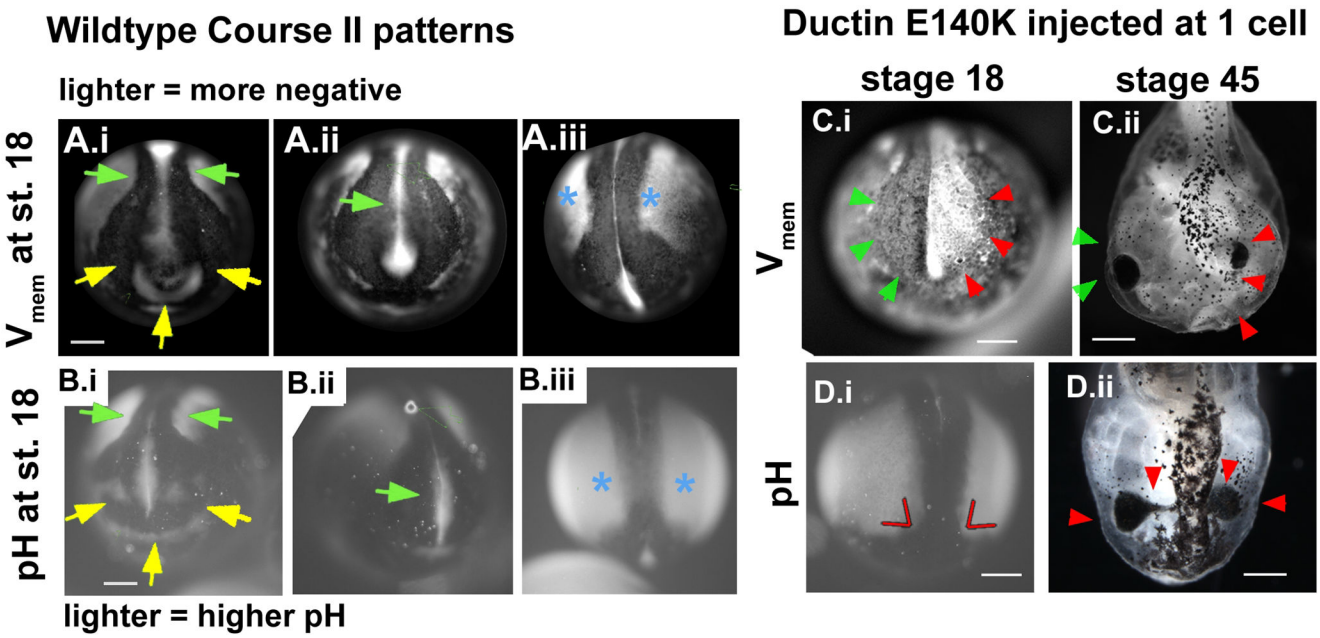

Figure 7. Inhibition of ductin causes changes in voltage patterns that correlate with CF phenotypes.

(**A**) Stills of wildtype embryos showing the pattern of V_{mem} in the anterior and antero-dorsal regions of neurulae at approximately stage 18. Arrowheads point to the most consistent features of the pattern (11 of 11 uninjected embryos). (**A.i**) Green arrows point to depolarized neural folds. Yellow arrows point to hyperpolarization in the future olfactory/oral region. (**A.ii**) Green arrow points to the disappearing signal from the neural tube floor. (**A.iii**) Blue asterisks mark hyperpolarized ectodermal regions lateral to the neural folds. (**B**) The pattern of pH in the anterior and antero-dorsal regions of untreated neurulae. Arrowheads point to features of a normal pattern, and are the same as V_{mem} shown in A. (**C, D**) Abnormal regionalization of V_{mem} and pH caused by injection of *xduct-noTM4.* (**C.i**) Abnormal V_{mem} patterns were seen in 9 of 13 injected embryos. Green arrowheads point to the normal depolarized neural folds, red arrows to the abnormal hyperpolarized side. (**D.i**) Red lines indicate the abnormal angle between the high pH lateral ectoderm and the low pH anterior folds. (**C.ii, D.ii**) The same embryos imaged at stage 45 display gross malformations (red arrows) in the areas with abnormal V_{mem} or pH.

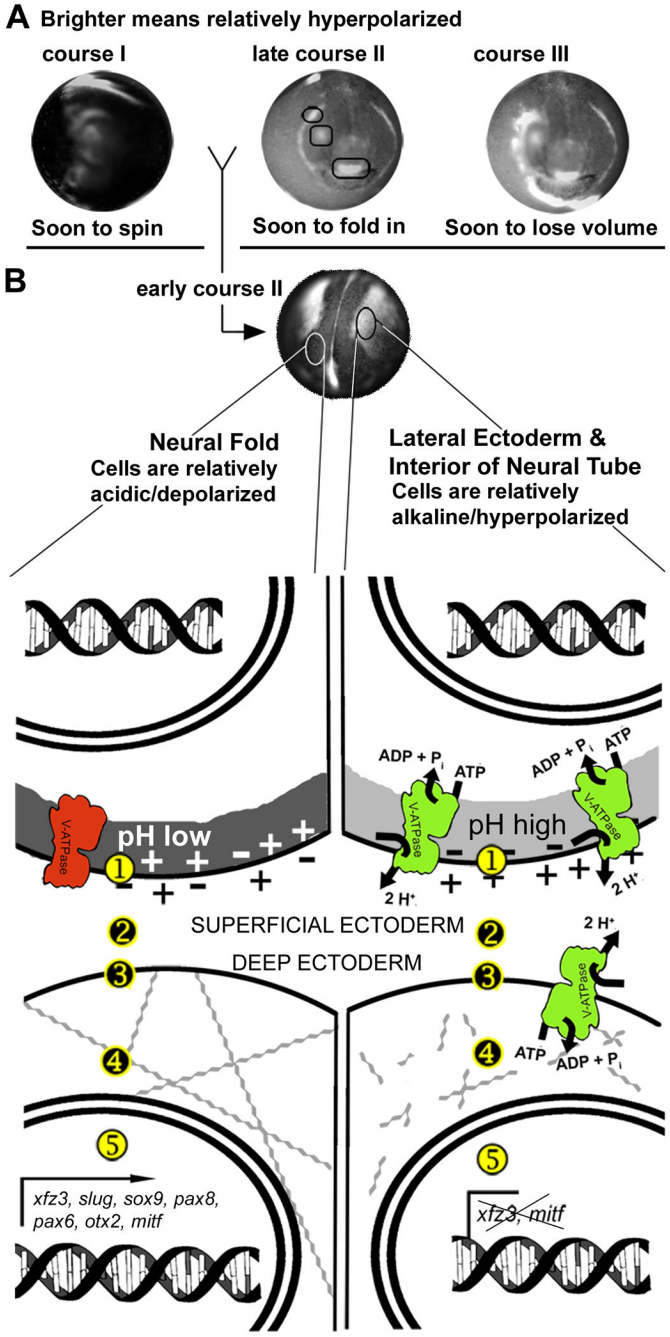

Figure 8. Summary model of Vmem/pH dependent signaling.

(**A**) The three courses of electrophysiological activity (Fig. 2). At approximately stage 18, a consistent pattern appears: depolarized neural folds (darker), hyperpolarized lateral ectoderm (brighter). (**B**) A typical wildtype stage 18 embryo. The pattern shown here for V_{mem} compartments matches the pattern seen for pH compartments at the same stage. Drawings illustrate our model. The V_{mem} and pH of the SE cells, labeled ① in the drawing, influence gene expression in the nearby deep cells, labeled ⑤. The electrophysiological state of the SE cell can influence the genes of the deep cell by various mechanisms, (①, ②, ③,

and ④). Secretion of signaling molecules can be affected by the H^+-V-ATPase-dependent control of vesicle pH (①), consistent with Cruciat (2010). Proteins on the surface of the SE cell (②) can be voltage or pH gated; many only function in a narrow range of pH or V_{mem}. The pH of the intercellular space (②), would also affect diffusible signaling molecules, or the receptors on the surface of the deep cells (③), by the same mechanism. After reaching the surface of the deep cell, the signal could be carried to the nucleus by any of a myriad of signaling pathways. We also hypothesize that the bioelectric signal originating in the SE cells affects the mechanical state of the cells. One hypothesis is that changes in V_{mem} open voltage-gated Ca^{2+} channels (③), leading to Ca^{2+}-dependent changes in the cytoskeleton (④), an important player in cell shape change and invagination. Another possibility is that V_{mem} changes trigger voltage gated ion channels (③), causing ion and thus water efflux, changing the osmotic pressure of the cells, and thus their resistance to shape change. This is consistent with our observation that cells expressing abnormally high amounts of *xfz3* often appear larger.

Table 1.

Percent of injected embryos with craniofacial phenotypes (CFPs) grouped by timing of injection.

1/1 = One cell injected of one cell embryo, 1/4 = one cell of four cell embryo, etc. Data is also presented to demonstrate the toxicity of each construct; the percentage shown indicates the number of unscorable embryos.

Treatment	Timing/Target	Uninjected controls % CFPs (n)	Injected % CFPs (n)	X^2	p	Toxicity of injected construct
nhe3	1/1	4% (77)	13% (136)	3.8	=0.050	15%
pma1.2	1/1 and 2/1	8% (147)	25% (175)	14.9	<0.001	12%
xduct-noTM4	1/1	3% (239)	28% (493)	16.5	<0.001	
	1/2	0% (60)	17% (64)	5.1	=0.024	29%
	1/4	3% (61)	37% (30)	15.7	<0.001	
xduct (wildtype)	1/2	2% (288)	44% (280)	136.2	<0.001	35%

Table 2.

mRNAs used.

Five mRNAs were used to vary H^+-flux. Eight mRNAs were used for in situ hybridization. Column 2 gives information about the protein product. Column three in the top half indicates the known or predicted effect of the protein. LOF=loss-of-function, GOF=gain-of-function.

mRNAs	Comments		Reference
nhe3	Sodium-hydrogen exchanger; increases H^+-efflux across plasma membrane	GOF	Praetorius et al., 2000
pma1.2	Single subunit yeast proton pump; increases H^+-efflux	GOF	Masuda and Montero-Lomeli, 2000
xduct	Proton binding subunit c of H^+-V-ATPase; may enhance H^+-V-ATPase	unknown	this article
xduct-noTM4	Ductin lacking the 4^{th} transmembrane domain; inhibits H^+-V-ATPase	LOF	this article
xduct-YFP	YFP tagged *xduct*; inhibits H^+-V-ATPase	LOF	this article
In situ Hybridization Probes			
mitf	Marks pre-migratory melanoblasts		Kumasaka et al., 2004
otx2	Marks anterior neural tube and eye primordium		Wu et al, 2006
pax6	Marks optic placodes, retina, and parts of the developing brain		Hirsch and Harris, 1997
pax8	Marks otic placode and presumptive pronephros		Saint-Germain et al., 2004
slug	Marks migrating neural crest cells		Carl et al., 1999
sox9	Marks neural crest forming regions and prospective otic placode		Saint-Germain et al., 2004
xfz3	Marks anterior neural folds, midbrain, optic and otic vesicles		Shi et al., 1998
xnr1	Marks left side of neurula		Sampath et al., 1997